Resistive switching near electrode interfaces: Estimations by a current model

Herbert Schroeder, Alexander Zurhelle, Stefanie Stemmer, Astrid Marchewka, and Rainer Waser

Citation: Journal of Applied Physics **113**, 053716 (2013); doi: 10.1063/1.4789944
View online: http://dx.doi.org/10.1063/1.4789944
View Table of Contents: http://scitation.aip.org/content/aip/journal/jap/113/5?ver=pdfcov
Published by the AIP Publishing

Resistive switching near electrode interfaces: Estimations by a current model

Herbert Schroeder,[1] Alexander Zurhelle,[2] Stefanie Stemmer,[2] Astrid Marchewka,[2] and Rainer Waser[1,2]
[1]*Institut Elektronische Materialien im Peter-Grünberg-Institut (PGI-7) and JARAFIT—Jülich Aachen Research Alliance Fundamentals of Future Information Technology, Forschungszentrum Jülich GmbH, D-52425 Jülich, Germany*
[2]*Institut für Werkstoffe der Elektrotechnik 2 (IWE-2), RWTH Aachen University, D-52074 Aachen, Germany*

(Received 12 September 2012; accepted 15 January 2013; published online 7 February 2013)

The growing resistive switching database is accompanied by many detailed mechanisms which often are pure hypotheses. Some of these suggested models can be verified by checking their predictions with the benchmarks of future memory cells. The valence change memory model assumes that the different resistances in ON and OFF states are made by changing the defect density profiles in a sheet near one working electrode during switching. The resulting different READ current densities in ON and OFF states were calculated by using an appropriate simulation model with variation of several important defect and material parameters of the metal/insulator (oxide)/metal thin film stack such as defect density and its profile change in density and thickness, height of the interface barrier, dielectric permittivity, applied voltage. The results were compared to the benchmarks and some memory windows of the varied parameters can be defined: The required ON state READ current density of 10^5 A/cm^2 can only be achieved for barriers smaller than 0.7 eV and defect densities larger than 3×10^{20} cm^{-3}. The required current ratio between ON and OFF states of at least 10 requests defect density reduction of approximately an order of magnitude in a sheet of several nanometers near the working electrode. © *2013 American Institute of Physics*. [http://dx.doi.org/10.1063/1.4789944]

I. INTRODUCTION

In the last decade the resistive switching phenomena have drawn tremendous attention and the increasing data pool has been reviewed frequently, e.g., Refs. 1–5. The switching properties of various material combinations in metal/insulator/metal (MIM) thin film stacks make them promising candidates for application as future non-volatile memory cells, called redox-based resistive random access memory (ReRAM) or memristive device,[6] and possibly substituting DRAM and/or FLASH. Typically, the insulator is a metal oxide. Together with the numerous experimental results many models and mechanisms are offered to explain the observed switching properties. A lot of them are postulating detailed working mechanisms even down to atomic scales, e.g., Refs. 7–10. It should be mentioned that several of them are (pure) hypotheses, not backed by any detailed microscopic investigations as these are very scarce (and in part inconclusive!).[11]

At present the most frequently used model assumes a so-called active electrode (e.g., Pt or TiN) and a highly conducting volume in the oxides. This may extend over the entire cross section of the cell in the so-called area-dependent type switching, or it is called filamentary type switching if its cross section area is much smaller than the electrode area.[1] In any case, this highly conducting volume is ending at an ohmic counter electrode. The highly conducting volume is typically created by a so-called electroforming process which is a voltage-induced reduction process in this model leading to a relatively high conductivity of a mixed electronic and ionic nature, defined as ON state. In the OFF state of the switch, a few nanometer thin sheet in the oxide is assumed between the active electrode and the highly conducting volume resulting in a higher resistance of the cell. The bipolar switching model describes the switching by the injection of positively charged, mobile ions (i.e., donors, such as oxygen vacancies (V_O)) from the highly conducting volume into this thin sheet at a negative voltage polarity at the active electrode, resulting in a lower ON state resistance due to the change in the average valence of the cation sublattice (hence the name valence change memory, VCM, for this mechanism). At the opposite polarity, the donors are driven back into the highly conducting volume of the oxide which restores the OFF state. These WRITE processes can be very fast due to a temperature and field acceleration at sufficiently high voltages,[10] while at lower voltages the resistance state can be read without affecting its resistance.

For some of the proposed models simple estimations can demonstrate the chances for realization by using the minimum requirements for future memory cells defined, e.g., by the International Technology Roadmap for Semiconductors, ITRS.[12] It has been demonstrated, e.g., for the "pure electronic" switching models that these mechanisms cannot work because of the "voltage-time dilemma," i.e., the incompatibility between the long retention time (10 years) and the short WRITE/READ current pulses ($t_{WRITE/READ} \leq 100$ ns) at high current densities and low applied voltages (≤ 1 V).[13]

In this paper, we will present such estimations for the READ currents in the ON and OFF states for the switching model described above. As input numbers we are using

updated benchmark data of the ITRS roadmap with a state-of-the-art memory area: A current density for the ON state to be detectable ($\geq 10^{-6}$ A/cell area) with a maximum cell area ($\leq 30\,\text{nm} \times 30\,\text{nm} \approx 10^{-11}$ cm^2) in future generations making the READ current density $\geq 10^5$ A/cm^2 (this value has to be adjusted, if the contributing cell area is different from the assumed number, and also, if, e.g., not the complete cell area is contributing to the current in the same way due to inhomogeneities of important parameters); an ON/OFF READ current ratio ≥ 10 at low READ voltage (0.1… 0.5 V); limited oxide thickness ($t_I \leq 30$ nm) in the MIM stack. In our current simulation model the different ON and OFF states are characterized by different defect densities in the thin sheet at the active electrode as schematically sketched in Fig. 1.

In the ON state a homogeneous defect density profile, N_D, is assumed throughout the oxide of thickness t_I, while the inhomogeneous profile in the OFF state most simply can be approximated by a constant, but reduced defect density, $N_{DS} < N_D$, in a narrow sheet of certain width $a_{DS} \ll t_I$ adjacent to the active electrode, making a "trench" in the defect density profile at one interface (Fig. 1(a)). These different defect profiles induce different barriers at the active electrode interface and different band profiles close to the interface via the different available space charge densities of the ionized defects in this region and the corresponding internal fields (Fig. 1(b)). These result in a lower barrier by the implemented image force for the injected electrons, the so-called "Schottky effect," and a much smaller screening length via steeper band bending due to the Poisson equation for the ON state compared to the OFF state expecting higher READ currents in the ON state. By using an appropriate current simulation model, one can estimate the currents through the MIM stack in the different states.

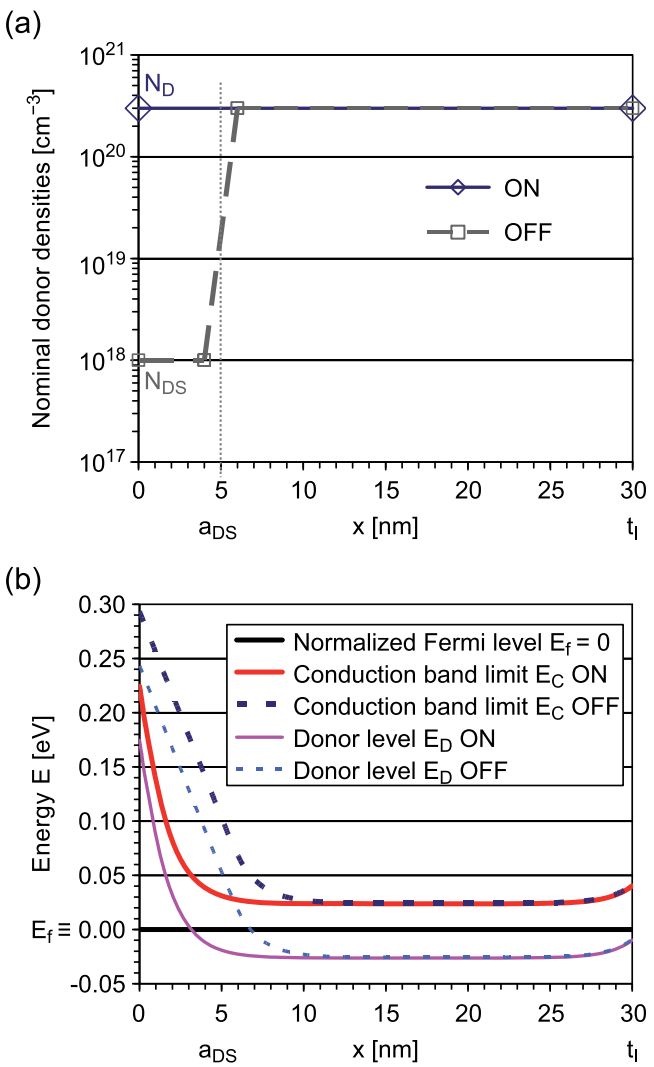

FIG. 1. (A) Nominal donor densities in ON and OFF states for simulations with the standard parameters (see also Table I). (b) Corresponding energies at zero applied voltage in ON and OFF states, respectively: Fermi level E_f (set to 0 eV), conduction band minimum E_C, and donor level, E_D.

The aim of this paper is to define parameter ranges of defect and material properties (such as the donor density in the ON state, N_D; the width of the sheet, a_{DS}, and its reduction in the defect density profile change, N_{DS}, for the OFF state; the electrode barrier height, Φ_B; the electron mobility, μ_e, permittivity, ε_r, and thickness, t_I, of the resistive insulator (oxide) material) to comply with the requirements defined by the benchmark values, i.e., to define working memory window parameters under the assumption of the postulated model.

II. SIMULATION TOOL AND VARIATION OF PARAMETERS

In order to calculate the steady state current density through the MIM stack, we have used a simulation tool with a self-consistent combination of injection/ejection current densities at the two MI interfaces, described by thermionic field emission (including the "Schottky effect"), and the drift-diffusion current density equation inside the oxide, described as a wide band gap semiconductor. The details of this simulation tool have been specified and published previously.[14–16] As an example for the switching, the most prominent defects in metal oxide, i.e., V_O, have been chosen as the defects with changing density profile in the thin sheet at the active electrode, acting as very shallow donors (0.05 eV below the conduction band, see Fig. 1(b)) with a double positive elementary charge, if ionized (V_O^{++}). After density profile rearrangement (switching)[10] the ionic defects are supposed as immobile. The densities of electronic and ionic charges are calculated using Fermi-Dirac statistics. Due to the assumed high densities of these shallow donors (N_D, $N_{DS} \geq 10^{18}$ cm^{-3}) and the relative low barriers at the injecting electrode ($\Phi_B \leq 1$ eV at zero applied voltage) the currents are exclusively dominated by electron conduction with negligible contributions of holes in a wide band gap semiconductor (band gap $E_g \approx 3$ eV). Hence, only parameters for electrons are considered in Table I and below. For calculation reasons the "trench" limit of the reduced defect density, N_{DS}, was not abrupt within the oxide at $x = a_{DS}$, but was smeared out in a range of 2 nm around a_{DS} with exponentially increasing profile (see Fig. 1(a)). Such a profile is also more realistic if the defect density change is controlled by external forces such as electric field.

The parameters varied for the investigated simulation range are listed in Table I. For the variation of a single

TABLE I. Variation range of important simulation parameters and their "standard" numbers.

Parameter	Variation range	"Standard" number
Thickness of oxide t_I [nm]	30–250	30
Thickness of switching sheet a_{DS} [nm]	0–10	5
Mobility μ_e [cm^2/Vs]	0.1–10	1.6
Relative permittivity ε_r	10–300	30
Barrier height at active electrode Φ_B [eV]	0.4–1.0	0.4
Applied voltage at active electrode (cathode) [V]	0.1–0.5	0.5
Homogeneous donor density N_D [cm^{-3}]	10^{18}–10^{21}	3×10^{20}
Reduced donor density N_{DS} in sheet a_{DS} [cm^{-3}]	10^{18}–N_D	10^{18}

parameter the others had some "standard" numbers, also listed in Table I. Other parameters have been kept constant, e.g., the effective density of states in the conduction band, $N_{DOS} = 3.5 \times 10^{20}\,cm^{-3}$, the effective Richardson constant for thermionic emission, $A^* = 980\,A/cm^2\,K^2$, which are numbers of the model oxide, $SrTiO_3$ (STO),[16] and the barrier height at the non-active electrode, nominally 0.1 eV (quasi-ohmic). All the simulations have been performed for room temperature (RT = 300 K) and a polarity of the applied voltage defining the active electrode as cathode.

III. RESULTS AND DISCUSSION

The most important benchmarks for the use of the switching MIM stack as a ReRAM are the unambiguous detection of the different states ON and OFF requiring an minimum current density of $10^5\,A/cm^2$ for the ON state (see Fig. 2) and an ON/OFF current ratio of at least 10 (see Figs. 3 and 4)!

Fig. 2 presents simulated current densities at 0.5 V applied voltage dependent on the relative permittivity of the

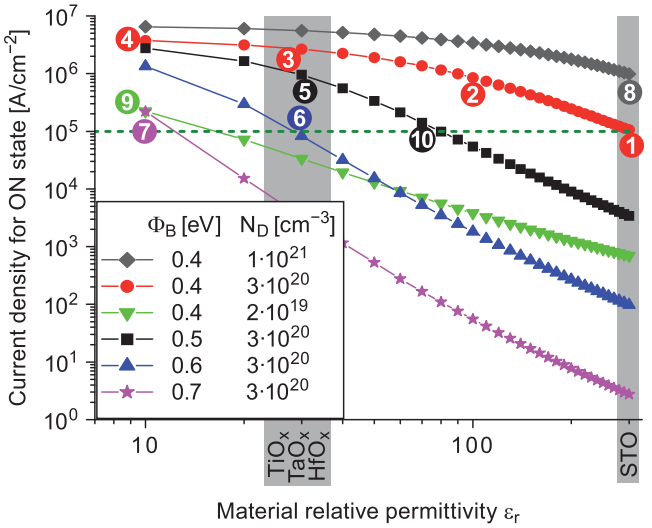

FIG. 2. Current densities in ON state dependent on relative permittivity, ε_r, for different injection barrier heights at cathode, Φ_B, and nominal donor densities, N_D. The (green) dashed line is the detection limit for the ON state ($>10^5\,A/cm^2$ benchmark value). The parameter sets for the indicated numbers are listed in Table II. Other parameters are standard: total thickness of oxide, $t_I = 30$ nm; thickness of switchable denuded zone at injection interface (cathode), $a_{DS} = 5$ nm; applied voltage, $V_{appl} = 0.5$ V; RT.

TABLE II. Number (#) and corresponding parameters of sets investigated in detail.

#	N_D [cm^{-3}]	Φ_B [eV]	ε_r	#	N_D [cm^{-3}]	Φ_B [eV]	ε_r
1	3×10^{20}	0.4	300	6	3×10^{20}	0.6	30
2	3×10^{20}	0.4	100	7	3×10^{20}	0.7	10
3	3×10^{20}	0.4	30	8	1×10^{21}	0.4	300
4	3×10^{20}	0.4	10	9	2×10^{19}	0.4	10
5	3×10^{20}	0.5	30	10	3×10^{20}	0.5	70

oxide for different nominal interface barriers at the active electrode and different nominal homogeneous defect densities for the ON state. For all the curves the current densities increase with decreasing dielectric constant, which is an effect of the Poisson equation: The available space charge is more effective with decreasing dielectric constant (in the denominator) resulting in higher internal electric fields and reduced screening lengths leading to higher current densities for the same reasons as above for Fig. 1. For the most interesting permittivity range, 10–300, only the data points with lowest barrier in the simulations, 0.4 eV, and high defect densities, $\geq 3.3 \times 10^{20}\,cm^{-3}$, are all above the benchmark value of $10^5\,A/cm^2$ for the READ current density. For higher barriers and/or lower defect densities the current densities are above the benchmark line only in the lower permittivity range. For the barrier/defect density pairs 0.4 eV/$2 \times 10^{19}\,cm^{-3}$ and 0.7 eV/$3.3 \times 10^{20}\,cm^{-3}$ the limit is reached only for the lowest permittivity, $\varepsilon_r = 10$. Therefore, a barrier height of nominally 0.7 eV is the upper limit, because at low permittivity the current increase with even higher defect density is not significant as concluded by the data with barrier 0.4 eV. This makes the barrier window quite narrow, 0.4–0.7 eV, reducing the number of possible electrode materials. For the most favorable materials for ReRAMs such as TiO_x, TaO_x, or HfO_x (Ref. 12) with permittivities around $\varepsilon_r \approx 30$ this window is even smaller. Materials with higher permittivity, such as STO with $\varepsilon_r = 300$, are usable only for the lowest barrier height of 0.4 eV. Reducing the READ voltage to only 0.1 V compared to 0.5 V, advantageously for energy saving, would reduce the shown current densities by almost an order of magnitude and therefore would shrink the barrier window further.

In order to investigate the dependencies of the OFF state current on variations of the numbers defining the switching sheet, i.e., depth N_{DS} (reduced defect density) and width a_{DS} of the "trench," some parameter sets were selected (see Table II) for which the benchmark for the ON state current density was fulfilled: Systematic variations of the permittivity (#1 to 4) and the barrier height (#3, 5, 6) as well as some other limiting cases (#7 to 10). The results are presented in Figs. 3 and 4.

The dependence of the OFF current, normalized to the ON current (for this ratio the benchmark is $j_{OFF} / j_{ON} \leq 0.1$) on the ratio N_{DS}/N_D (=1 represents the homogeneous ON state) is demonstrated in Fig. 3 with $N_{DS} = 1 \times 10^{18}\,cm^{-3}$ as lower limit. As a general trend all the curves saturate to a lower limit for the current ratio when approaching the N_{DS} limit indicating little effect by further increasing the depth of

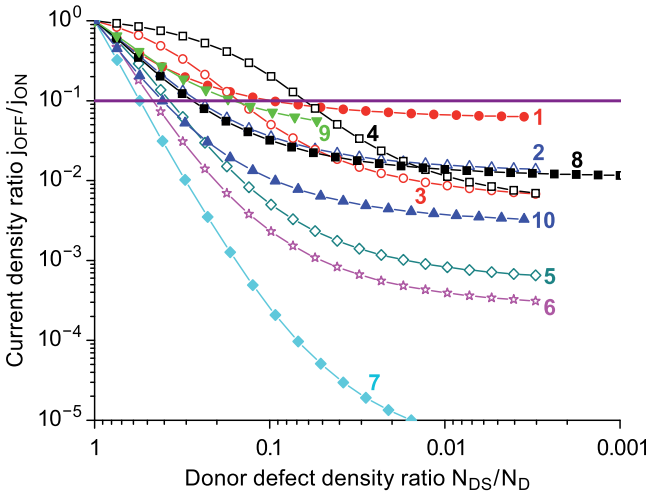

FIG. 3. Ratio of current densities in OFF state and ON state, j_{OFF}/j_{ON}, dependent on the ratio of the reduced donor density in the switchable denuded zone, N_{DS} [cm^{-3}], and the homogeneous donor density, N_D [cm^{-3}], for selected combinations (see # in Table II) of donor density, N_D [cm^{-3}], barrier height at injecting electrode (cathode), Φ_B°[eV], and relative permittivity, ε_r. The (purple) full horizontal line is the detection limit for the j_{OFF}/j_{ON} ratio ($\leq$ 0.1 benchmark value). Other parameters are standard: total thickness of oxide, $t_I = 30$ nm; thickness of switchable denuded zone at injection interface (cathode), $a_{DS} = 5$ nm; applied voltage, $V_{appl} = 0.5$ V; RT.

the trench. Another trend is that the benchmark line is crossed at lower donor density ratios for increasing barrier height due to steeper curves indicating an increased current reduction at the same density reduction. The minimum reduction of the defect density in the switching sheet to be consistent with the benchmark starts from a factor of 2 (#7) to more than an order of magnitude (#1, 4). The steepest curve (#7) would also allow multiple different states if the reduced defect density in the switching sheet could be controlled precisely. If this control cannot be achieved the steepness may be disadvantageous, if the switching ratio should be kept in a certain range, e.g. the OFF/ON ratio between 1/10 and 1/100. The dependence on permittivity (#1-4) is less systematic on a first glance because the shape of the curves is changing: While at higher permittivity the curves have always the same curvature, this changes for lower permittivity for which at high density ratios the current ratio decrease is much smaller resulting in a different curvature with an inflection point shifting to lower defect ratios with decreasing permittivity. As a result the benchmark line is crossed by the curve with $\varepsilon_r = 10$ (#4) at lower density ratios than all other curves including the one with $\varepsilon_r = 300$ (#1).

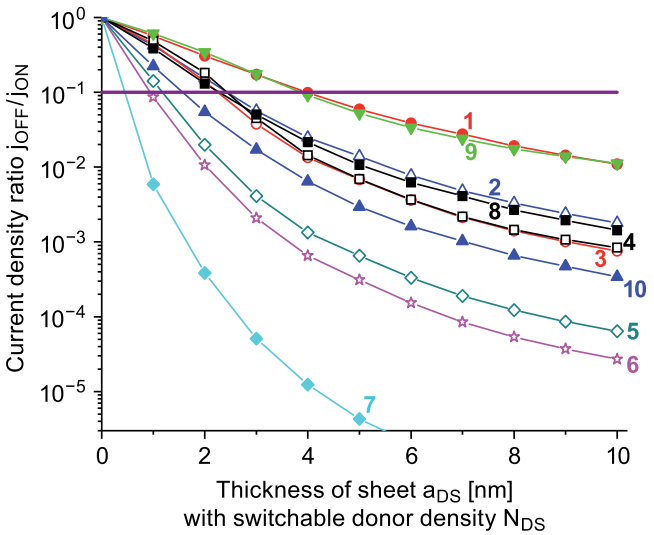

FIG. 4. Ratio of current densities in OFF state and ON state, j_{OFF}/j_{ON}, dependent on the thickness of the switchable denuded zone, a_{DS}, with $N_{DS} = 1 \times 10^{18}$ cm^{-3} at cathode for selected combinations (see # in Table II) of homogeneous donor density, N_D [cm^{-3}], barrier height, ε_B [eV] at injecting electrode (cathode), and relative permittivity, ε_r. The full (purple) horizontal line is the detection limit for the j_{OFF}/j_{ON} ratio ($\leq$0.1 benchmark value). Other parameters are standard: total thickness of oxide, $t_I = 30$ nm; applied voltage $V_{appl} = 0.5$ V; RT.

Another important parameter usually not known in the models (and corresponding experiments) is the width a_{DS} of the depleted trench at the active interface. In all the presented data (Figs. 2 and 3), this width had the standard value of 5 nm. Data with varying sheet thickness, a_{DS}, are presented in Fig. 4 for the same parameter sets as in Fig. 3 with fixed trench depth, $N_{DS} = 1 \times 10^{18}$ cm^{-3}, the low standard number: To satisfy the benchmark ratio (j_{OFF} / $j_{ON} \leq 0.1$) all the curves show a minimum trench width, increasing with decreasing barrier height and increasing relative permittivity, from about 0.6 nm for the high barrier/low permittivity curve (#7) to about 4 nm for the lower barrier/high permittivity and lower barrier/low defect density curves (#1 and 9, respectively). The sequential order of the curves is conserved over the whole range of varied a_{DS}. At constant barrier height (0.4 eV) lower or higher permittivity can be made up by changing N_D for about the same factor (#1 and 9). In order to control the OFF/ON ratio in a certain limited band, once more it is more difficult for the curve with the most attractive low sheet thickness (#7) because of the high steepness of that curve compared to the others, but on the other hand a precise control of the width of the reduced density sheet would allow for multiple states.

Other varied parameters listed in Table I are the thickness of the oxide, t_I, and its electron mobility, μ_e. As the total oxide thickness larger than 30 nm had a minor influence in the ON state for all defect densities, which is due to the low barriers and high defect densities of very shallow donors making the screening length to near equilibrium state in the oxide much shorter than 30 nm (see Fig. 1(b)), and thicker oxide films are not so important for future memory generations anyway, all the other parameter variations were done for a fixed $t_I = 30$ nm only. A variation of the electron mobility by two orders of magnitude changed the ON state current density by about a factor of ten. As the influence on the current in the OFF state was nearly identical, also this parameter was kept constant. The temperature would have a larger influence on the absolute value of the current densities, increasing with increasing temperature.

The difference of the current densities in ON and OFF states can be exemplified by the simulation data with the parameter numbers of set #1. The densities of ionized defects (donor charge) and the conduction electrons are shown in Fig. 5. It is most striking that in the region near the active electrode (left) the charges are far from their equilibrium

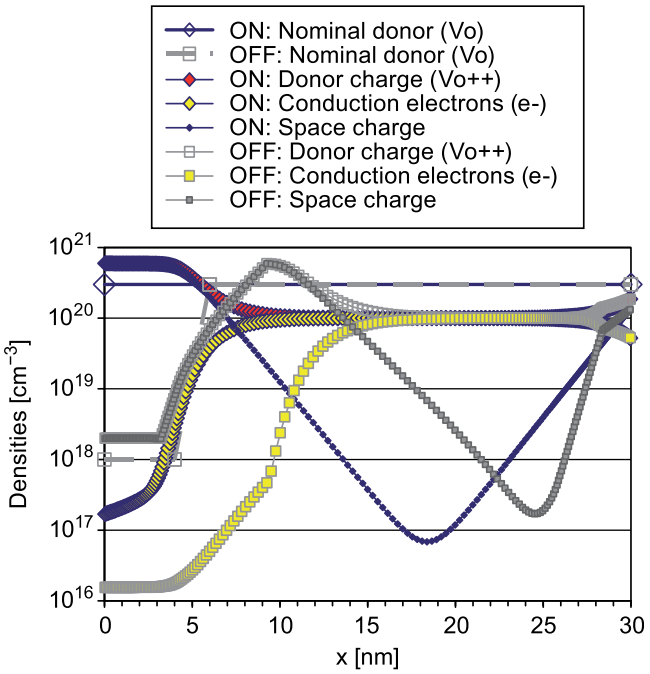

FIG. 5. Densities in ON and OFF states for simulations with the standard parameters (see also Table I): Nominal defects (V_O; see Fig. 1(a)); ionized donor charges (V_O^{++}), conduction electrons (e^-), and resulting space charge densities for an applied voltage $V_{appl} = 0.5$ V.

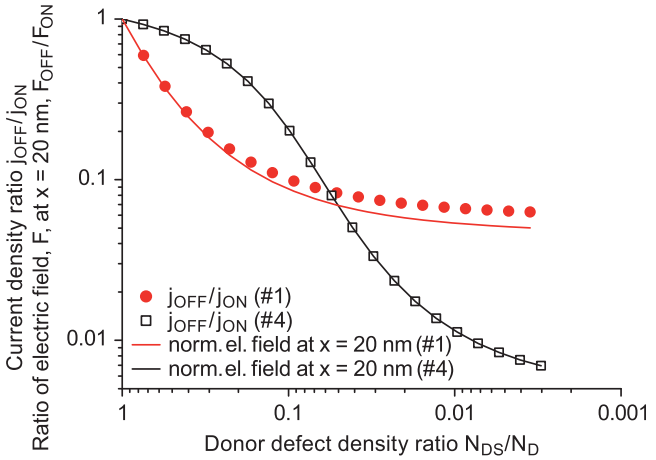

FIG. 6. Correlation between current density ratio j_{OFF}/j_{ON} (data points) and corresponding ratio of electric field, F, at x = 20 nm, F_{OFF}/F_{ON} (full lines), plotted vs. ratio of donor defect densities, N_{DS}/N_D (same as in Fig. 3).

values which are established in the right middle part of the oxide (between approx. 15 and 25 nm) and is characterized by a density of about 10^{20} cm^{-3} for positive (V_O^{++}) and negative (e^-) charges, respectively. Of course, this region near equilibrium is almost electrically neutral (with much smaller space charge, down to a minimum of 10^{17} cm^{-3}). The Fermi-level, E_F, in this region is above the donor level ($E_D = -0.05$ eV below E_C), approximately in the middle between this value and the conduction band minimum, E_C, at $E_F \approx -0.025$ eV (see Fig. 1(b)). Therefore, only about 16% of the oxygen vacancies are ionized and due to the small distance of E_F from E_C the electron density is very high in this region, $n_e \approx 10^{20}$ cm^{-3}, giving rise to high current densities ($>10^5$ A/cm^2 for ON state) at moderate electric fields (for the ON state: about 5 kV/cm compared to mean applied electric field, 167 kV/cm) due to the dominant voltage drop in the left part of the oxide.

In this part near the active electrode there are significant differences for ON and OFF states. Due to the barrier at the active electrode (nominally at 0.4 eV), all the available donor defects are ionized while the electronic charge density is quite small giving much higher positive space charge density for the ON state than for the OFF state ("trench" at the (left) interface) proportional to the defect density in that region. This has two main consequences: Firstly, the much higher space charge induces a much higher internal electric field reducing the barrier via the Schottky-effect to an effective value of 0.17 eV for the ON state compared to 0.24 eV for the OFF state in the shown example. For the ON state this increases both the electron injection current at the active electrode and the starting electron density at the interface, as demonstrated in Fig. 5. And secondly, the much higher space charge reduces the screening length to reach the near-equilibrium state, which is established already from x ≈ 8 nm for the ON state compared to x ≈ 15 nm for the OFF state. These differences account for the much larger voltage drop (or higher resistance) in this region for the OFF state, so that much less voltage remains in the equilibrium region for the OFF state. All these effects result in a more than 10 times higher steady state current density in the ON state (see Fig. 3, #1) for this parameter set.

All other presented simulation data with different parameters can be explained with similar arguments: Decreasing permittivity and increasing defect density increase the internal fields near the active electrode making the barrier and the screening length smaller and thus inducing higher current densities (see Fig. 2). Increasing ratio of N_D/N_{DS} (Fig. 3) and increasing trench width a_{DS} (Fig. 4) increase the differences of space charge and internal field between ON and OFF state and make the current density ratio ON/OFF larger.

The unusual behavior of the curves #1–4 in Fig. 3 can be explained with the help of Fig. 6. The current through the MIM stack can be correlated to the electrical field strength, F, in the quasi-equilibrium region in the right part of the oxide (see Figs. 5 and 1(b)) in which the electron density is about constant and identical for all cases. Also, the influence of space charge and thus internal fields is only marginal. As shown in Fig. 6 for the curves #1 and 4 the normalized electric field, F_{OFF}/F_{ON}, in this region (at x = 20 nm) correlates quite perfectly to the normalized current density (see also Fig. 3). It can be concluded from this correlation, that the voltage drop (or resistance) for curve #4 in the trench region near the active interface increases more slowly with decreasing defect density in the OFF state at high ratios N_{DS}/N_D compared to curve #1, so that the available voltage drop and the corresponding electrical field in the quasi-equilibrium is higher for curve #4 than for #1 in this defect ratio region. This effect is made by a complicated interplay of several effects dependent on the very different permittivities, 10 for #4 and 300 for #1, respectively, but can be explained by the shown simple correlation.

IV. SUMMARY AND CONCLUSIONS

The ambitious benchmarks for ReRAM make the memory window for all materials rather challenging: For the most favorable ones with $\varepsilon_r \approx 30$ the barrier at the active electrode has to be $\Phi_B \leq 0.6\,eV$ with defect densities $N_D \geq 3 \times 10^{20}\,cm^{-3}$ to comply with the benchmark for the ON state. For high permittivity materials such as STO ($\varepsilon_r \approx 300$), this barrier limit decreases to about $\leq 0.4\,eV$ making the selection of appropriate electrode materials more difficult. For lower defect densities or higher barriers within a rather limited range ($N_D \geq 2 \times 10^{19}\,cm^{-3}$ or $\Phi_B \leq 0.7\,eV$), only materials with very low ε_r are suitable.

For the OFF state the combined standard numbers for the trench depth and width, $N_{DS} = 10^{18}\,cm^{-3}$ and $a_{DS} = 5\,nm$, respectively, are too conservative for most data sets. Less defect density reduction or smaller sheet thickness are possible to comply with the benchmark for the j_{ON}/j_{OFF} ratio: Except for the unusual curve #4 a defect density reduction of one order of magnitude or less, down to only a factor of 2 with $a_{DS} = 5\,nm$, satisfies the benchmark. A typical acceptable trench width is about 2 nm at $N_{DS} = 10^{18}\,cm^{-3}$ but this width would increase with higher reduced defect densities.

As the dependence of the results on oxide thickness is rather small, the presented data and conclusions should be applicable to a lower oxide thickness than 30 nm down to a value larger than the screening length to the quasi-equilibrium state. For the standard set this is approximately 15 nm.

ACKNOWLEDGMENTS

The authors would like to thank the Deutsche Forschungsgemeinschaft (DFG) for their financial support within the Sonderforschungsbereich (SFB) 917.

[1]R. Waser and M. Aono, Nature Mater. **6**, 833 (2007).
[2]A. Sawa, Mater. Today **11**, 28 (2008).
[3]R. Waser *et al.*, Adv. Mater. **21**, 2632 (2009).
[4]J. J. Yang *et al.*, MRS Bull. **37**, 131–137 (2012).
[5]R. Waser *et al.*, *Nanoelectronics and Information Technology*, 3rd ed. (Wiley-VCH, 2012), p. 683.
[6]J. J. Yang *et al.*, Nature Nanotechnol. **3**, 429 (2008).
[7]M. Fujimoto *et al.*, Appl. Phys. Lett. **89**, 223509 (2006).
[8]Z. Wei *et al.*, Tech. Dig. - Int. Electron Devices Meet. **2008**, 293.
[9]R. Meyer *et al.*, Proc. NVMTS **2008**, 54.
[10]S. Menzel *et al.*, Adv. Funct. Mater. **21**, 4487 (2011).
[11]H. Schroeder, R. Pandian, and J. Miao, Phys. Status Solidi A **208**, 300 (2011).
[12]See www.itrs.net for ITRS roadmap.
[13]H. Schroeder, V. V. Zhirnov, R. K. Cavin, and R. Waser, J. Appl. Phys. **107**, 054517 (2010).
[14]H. Schroeder, S. Schmitz, and P. Meuffels, Integr. Ferroelectr. **47**, 197 (2002).
[15]H. Schroeder, S. Schmitz, and P. Meuffels, Appl. Phys. Lett. **82**, 781 (2003).
[16]H. Schroeder and S. Schmitz, Appl. Phys. Lett. **83**, 4381 (2003).